

Efficient and improved prediction of the band offsets at semiconductor heterojunctions from meta-GGA density functionals

Arghya Ghosh,¹ Subrata Jana,^{2, a)} Tomáš Rauch,^{3, 4} Fabien Tran,⁵ Miguel A. L. Marques,^{6, 4} Silvana Botti,^{3, 4} Lucian A. Constantin,⁷ Manish K Niranjana,¹ and Prasanjit Samal⁸

¹⁾ *Department of Physics, Indian Institute of Technology, Hyderabad, India*

²⁾ *Department of Chemistry & Biochemistry, The Ohio State University, Columbus, OH 43210, USA*

³⁾ *Institut für Festkörpertheorie und -Optik, Friedrich-Schiller-Universität Jena, 07743 Jena, Germany*

⁴⁾ *European Theoretical Spectroscopy Facility*

⁵⁾ *VASP Software GmbH, Sensengasse 8, A-1090 Vienna, Austria*

⁶⁾ *Institut für Physik, Martin-Luther-Universität Halle-Wittenberg, 06120 Halle/Saale, Germany*

⁷⁾ *Istituto di Nanoscienze, Consiglio Nazionale delle Ricerche CNR-NANO, 41125 Modena, Italy*

⁸⁾ *School of Physical Sciences, National Institute of Science Education and Research, HBNI, Bhubaneswar 752050, India*

(Dated: 28 July 2022)

Accurate theoretical prediction of the band offsets at interfaces of semiconductor heterostructures can often be quite challenging. Although density functional theory has been reasonably successful to carry out such calculations and efficient and accurate semilocal functionals are desirable to reduce the computational cost. In general, the semilocal functionals based on the generalized gradient approximation (GGA) significantly underestimate the bulk band gaps. This, in turn, results in inaccurate estimates of the band offsets at the heterointerfaces. In this paper, we investigate the performance of several advanced meta-GGA functionals in the computational prediction of band offsets at semiconductor heterojunctions. In particular, we investigate the performance of r²SCAN (revised strongly-constrained and appropriately-normed functional), rMGGA (revised semilocal functional based on cusplless hydrogen model and Pauli kinetic energy density functional), mTASK (modified Aschbrock and Kümmel meta-GGA functional), and LMBJ (local modified Becke-Johnson) exchange-correlation functionals. Our results strongly suggest that these meta-GGA functionals for supercell calculations perform quite well, especially, when compared to computationally more demanding GW calculations. We also present band offsets calculated using ionization potentials and electron affinities, as well as band alignment via the branch point energies. Overall, our study shows that the aforementioned meta-GGA functionals can be used within the DFT framework to estimate the band offsets in semiconductor heterostructures with predictive accuracy.

I. INTRODUCTION

Over the past three decades, semiconductor heterostructure engineering has greatly influenced the development of nanoelectronic, optoelectronic, and other multifunctional devices^{1–5}. In recent years, the interest in heterostructures with atomically sharp interfaces has increased manifold due to their huge potential in advanced nanoscale technologies as well as the possibility of fascinating emergent interfacial phenomena in them^{6–9}. For instance, integer and fractional quantum hall effects have been discovered in high mobility two-dimensional electron gas formed at the interface of GaAs/AlGaAs heterostructures^{10–13}. The 2D topological insulator phase also exhibits quantum spin hall effect was first observed in quantum well heterostructures such as HgTe/CdTe^{14,15}.

One of the most important parameters in heterostructures is the band offset or band alignment at the interface. The band offset critically controls the out-of-plane electrical transport and capacitance behavior in heterostructure based devices. Naturally, the control and tunability of band offsets are highly desirable since it renders the control of the overall device performance and functionality^{1,2,5,16}. In general, the band offsets in heterostructures can critically depend on the interfacial atomic structure^{2,16–20}. Therefore, one way to control band offsets is via atomic level manipulation of the heterointerface^{16,20}. In this context, the accurate theoretical estimates and prediction of band offsets can be quite advantageous as these can guide the development and fabrication of heterostructures based devices. Over the years, ab-initio calculations based on the density functional theory (DFT)^{21–25} have been widely used to estimate the band offsets^{2,16,19,20}. Further, these past studies have been mostly performed within the local density approximation (LDA)²⁶ and/or semi-local generalized gradient approximation (GGA)^{27,28} functionals²⁹. However, the DFT calculations with GGA (LDA) functionals suffer from the

^{a)}Electronic mail: Corresponding author: subrata.niser@gmail.com

drawback to severely underestimate the band gaps^{30–38} and thereby the band offsets^{29,39,40}. Several earlier studies have suggested that band gap accuracy of semilocal GGAs is quite inadequate as compared to that of beyond-semilocal methods, like (system or dielectric-dependent) hybrid DFT^{41–52} or Green function based many-body calculations (GW method)^{53,54}. Though hybrids and GW calculations allow to calculate band gaps and band offsets closer to the experimental magnitudes^{29,55–57}, those methods are not computationally feasible for large supercell. Hence, as an alternative, the computationally efficient meta-generalized gradient approximations (meta-GGAs) functionals^{33,58–66} could be a good choice for estimating heterostructure band offsets, especially, as recent studies have shown that those can be applied reliably and in an improved way for obtaining the band gaps of bulk and layered solids^{32,38,64,65,67–69}. Recently, a methodology based on hybrid (HSE06) and GGA functional has also been proposed for estimating band offsets²⁹. In this method, bulk band structures are calculated using a hybrid functional(HSE). However, atomic relaxations and the potential alignment in the superlattice are calculated using the GGA functional which is highly less expensive computationally as compared to HSE. The present study is different from that presented in Ref.²⁹ in that entire supercell calculations are done using meta-GGA functionals.

In fact, motivated by those improved reliabilities for band gaps, in this paper we use meta-GGA functionals to study the band offsets at 14 semiconductor heterojunctions composed of Zincblende and diamond structures with (110) interfaces. We assess the performance of the functionals by considering both homovalent (e.g. GaAs/AlAs and GaP/AlP) and heterovalent heterojunctions (e.g., Ge/GaAs, Si/GaP, Ge/AlAs, ZnSe/GaAs, and Ge/ZnSe). We calculate the band offsets using (i) the ionization potential (IP)³⁹, (ii) the branch point energy (BPE), or charge neutrality level (CNL)^{5,70–75}, and (iii) the average potential in the supercell containing heterostructures^{1,29,40,76,77}.

At the meta-GGA level of approximation, we mainly focus on the r²SCAN⁶² (revised strongly-constrained and appropriately-normed (SCAN)⁵⁹), rMGGAC⁶³ (revised semilocal functional based on cusplless hydrogen model and Pauli kinetic energy density (MGGAC)⁶¹), mTASK⁶⁴ (modified Thilo Aschebrock and Stephan Kümmel (TASK)⁶⁵ functional), and LMBJ⁷⁸ (local modified Becke-Johnson (MBJ)⁷⁹) semilocal functionals. We have chosen the aforementioned recently proposed meta-GGAs instead of earlier proposed meta-GGAs (like Tao-Perdew-Staroverov-Scuseria⁸⁰) since these new functionals show considerable improvement for the band gaps of bulk and 2D layered materials^{32,64,65,67–69} and are therefore better suited for estimating the band offsets.

This paper is organized as follows. In sec. II, we briefly present the meta-GGA functionals considered in this study. In section III, we discuss all results. The conclusions are presented in Sec. IV.

II. BRIEF OVERVIEW OF METHODS

Here, we briefly discuss the exchange-correlation (XC) functionals considered this study, starting from the standard GGA-PBE functional²⁷. In general, the band gap estimates are not accurate enough when PBE is used. Nevertheless, since it is a widely used functional and its performance will serve as a reference for more accurate functionals. r²SCAN^{59,62} and rMGGAC^{61,63} are general purpose meta-GGA functionals. While r²SCAN is constructed by satisfying as many constraints as possible, rMGGAC satisfies fewer constraints. Also, the construction of r²SCAN is non-empirical, while some of the parameters of rMGGAC are fitted by using test sets. In fact, both functionals show improved performance to evaluate the band gaps of solids with respect to PBE^{35,36,62,63,81}. Unlike r²SCAN and rMGGAC, mTASK^{64,65} should not really be considered as a general purpose functional, but more specialized for the band gap of solids^{32,64,65,67–69}.

In addition to the XC approximations listed above, which are based on an energy functional, we will also consider the potential-only LMBJ⁷⁸ method. The MBJ XC potential is an improvement of the Becke-Johnson potential⁸² that in addition uses an average of the reduced density gradient $\frac{|\nabla\rho|}{\rho}$. While in MBJ the average of the reduced density gradient is calculated in the whole unit cell, in LMBJ it is local and calculated at every point of space, allowing for the application of the potential also to systems with vacuum and inhomogeneous materials⁷⁸. The LMBJ potential contains four parameters, and we chose the values $\alpha = 0.488$, $\beta = 0.5$ Bohr, $\sigma = 2$ Å, and $r_s^{\text{th}} = 7$ Bohr, based on previous optimizations^{83,84}. MBJ is currently the most accurate semilocal functional for the band gap of bulk solids^{32,67}, while LMBJ belongs to the group of accurate functionals for two-dimensional materials^{68,69}.

III. RESULTS AND DISCUSSIONS

In this paper, we calculate the band offsets using three different schemes, namely: (i) Ionization potential (IP) based, (ii) Branch-point energy (BPE) based, and (iii) Average potential (APM) based. The IP and BPE based methods involve calculation of bulk and surface components only. On the other hand, the APM requires calculation for entire superlattice. Therefore, the APM or average potential based calculations are typically the most expensive, followed by the IP-based and BPE-based ones. One may also note that the interface contribution to band offsets may only be estimated using average potential method as discussed later. In the following we briefly discuss these methods.

A. Ionization potential and electron affinity

We first define the ionization potential (IP), electron affinity (EA) and their connection with the band alignments of the heterostructure. For solids, the IPs are defined as the difference between the vacuum level of the electrostatic potential and the valance band maximum (VBM),

$$\epsilon_{\text{IP}} = [\epsilon_{\text{Vac},s} - \epsilon_{\text{Ref},s}] - [\epsilon_{\text{VBM},b} - \epsilon_{\text{Ref},b}], \quad (1)$$

where $\epsilon_{\text{Vac},s} - \epsilon_{\text{Ref},s}$ is calculated for the surface supercell constructed in the (110) direction (for the zincblende structure) taking into account the macroscopic average of the local electrostatic potential in the vacuum region ($\epsilon_{\text{Vac},s}$) and in the bulk region ($\epsilon_{\text{Ref},s}$) of the supercell. $\epsilon_{\text{VBM},b} - \epsilon_{\text{Ref},b}$ is determined from the bulk calculation, with $\epsilon_{\text{VBM},b}$ being the position of VBM and $\epsilon_{\text{Ref},b}$ the reference level for the bulk calculation, i.e., the average of the electrostatic potential in the unit cell. Then, the EAs are obtained using the formula $\epsilon_{\text{EA}} = \epsilon_{\text{IP}} - \epsilon_{\text{g}}$, where ϵ_{g} is the band gap of the bulk structure. The details of the calculation procedure of IPs and EAs are given in Section III D.

From IPs and EAs obtained for different semiconductors as described above, one can in principle extract the band offsets between two materials by comparing the differences between their IPs and EAs. To obtain the valance band offset (VBO) ($\Delta\epsilon_v$) between materials A and B, we evaluate

$$\Delta\epsilon_v = \epsilon_{\text{IP}}^{\text{B}} - \epsilon_{\text{IP}}^{\text{A}}. \quad (2)$$

It should be noted that this method neglects the effects occurring during the actual formation of the interface, such as charge transfer, interface dipole, or atomic relaxations. Still, it can be applied to interfaces of semiconductors with similar lattice constants where such effects are expected to be weak and can thus be neglected.

Finally, we did not calculate the IPs and EAs using the LMBJ potential, since some of us recently demonstrated in Ref. 85 that the band edges of semiconductors are predicted to be located too high with respect to the vacuum level by the LMBJ potential.

B. Band offsets from branch point energy

In the context of band alignment, another important quantity that serves as an energy reference level is the branch point energy (BPE)^{5,70–75}. The BPE can be approximated as the following averaging rule of high-lying valance bands (VB) and low-lying conduction bands (CB),

$$\epsilon_{\text{BPE}} = \frac{1}{2\mathcal{N}_k} \sum_k \left[\frac{1}{\mathcal{N}_{\text{VB}}} \sum_i^{\mathcal{N}_{\text{VB}}} \epsilon_i^v(\mathbf{k}) + \frac{1}{\mathcal{N}_{\text{CB}}} \sum_j^{\mathcal{N}_{\text{CB}}} \epsilon_j^c(\mathbf{k}) \right], \quad (3)$$

where \mathcal{N}_k is the number of \mathbf{k} points in the Brillouin zone, $\epsilon_i^v(\mathbf{k})$ and $\epsilon_j^c(\mathbf{k})$ denote the i^{th} highest VB and j^{th} lowest CB at wave vector \mathbf{k} , respectively. The sum over i and j runs over \mathcal{N}_{CB} lowest CBs and \mathcal{N}_{VB} highest of VBs. In Ref. 39, for the zincblende and diamond phases $\mathcal{N}_{\text{VB}} = 2$ and $\mathcal{N}_{\text{CB}} = 1$ was considered. Here, we include spin-orbit coupling in bulk calculations and we consider a (110) oriented bulk unit cell with four atoms. Therefore, we chose $\mathcal{N}_{\text{VB}} = 8$ and $\mathcal{N}_{\text{CB}} = 4$.

Finally, given the IP and BPE of two materials A and B, the VBO of the A/B heterojunction is calculated using the linear model^{75,86,87},

$$\Delta\epsilon_v = (\epsilon_{\text{IP}}^{\text{B}} - \epsilon_{\text{BPE}}^{\text{B}}) - (\epsilon_{\text{IP}}^{\text{A}} - \epsilon_{\text{BPE}}^{\text{A}}) + \mathcal{S}(\epsilon_{\text{BPE}}^{\text{B}} - \epsilon_{\text{BPE}}^{\text{A}}), \quad (4)$$

where \mathcal{S} is the dimensionless pinning factor⁷⁵. Following Ref. 74, the VBOs from the IP rule (see Eq. (2)) and BPE-matching rule corresponds to $S = 1$ and $S = 0$, respectively. In the latter, we substitute the IP with the VBM. Thus, $\epsilon_{\text{BPE}} - \epsilon_{\text{VBM}}$, which enters Eq. (4), can be obtained from a bulk calculation.

C. Band offsets from average potential method

To estimate the band offsets, we also consider the average potential method (APM). The band offset in this case is determined using the lineup of the local electrostatic potential in the supercell including the interface and the position of the VBM in bulk calculations of the materials A and B forming the interface. We calculate the VBO as^{29,76}

$$\Delta\epsilon_v = (\epsilon_{\text{VBM},b}^{\text{B}} - \epsilon_{\text{Ref},b}^{\text{B}}) - (\epsilon_{\text{VBM},b}^{\text{A}} - \epsilon_{\text{Ref},b}^{\text{A}}) + \Delta V, \quad (5)$$

where $\epsilon_{\text{VBM},b}^{\text{A/B}}$ is the VBM position and $\epsilon_{\text{Ref},b}^{\text{A/B}}$ the reference potential (unit cell average) of bulk material A/B. ΔV is the difference of the macroscopic averages of the electrostatic potential in the bulk-like regions of the A and B parts of the supercell. To obtain the average potential, we first calculate the in-plane average of the local potential and then obtain the macroscopic average from its Gaussian average. The macroscopic average is almost constant in the two bulk-like regions of the supercell. This method is different from the other methods discussed above in that it takes into account the atomic and electronic structure of the interface which may critically influence the band offset. It should be further noted that to evaluate band offsets from Eq. (5) we consider strained bulk structures, as described in Sec. III D. Thus, we calculate band offset for what is referred to here as strained interface⁷⁶.

From the accuracy point of view, the average potential method (APM) can be considered the “state-of-art” of band offset calculations, since it includes the effects of the interface atomic structure, such as the interface dipole. These are neglected in the BPE- and IP-based methods. Nevertheless, for lattice-matched heterostructures with no significant interface reconstructions, the

latter two methods can yield reasonable results. For lattice mismatched systems, the APM method should be chosen.

D. Calculation details

For benchmark calculations of band offsets, we consider in total 14 heterostructure interfaces between zincblende (*zb*) (AlAs, AlSb, CdTe, InSb, GaAs, GaP, ZnSe, and ZnTe) and diamond (Si and Ge) structures. We consider nonpolar (001) surfaces and interfaces, including the Si and Ge diamond structures. This set is chosen so that there is minimal strain at the interfaces³⁹.

We perform DFT calculations using the plane-wave code Vienna Ab-initio Simulation Package (VASP)^{88–91}. For Ga, Ge, and In, we used pseudopotentials with relatively deep Ga *3d*, Ge *3d*, and In *4d* states treated as valence orbitals. Surface calculations are performed on slabs consisting of 14 atomic layers (18 – 39Å) followed by 14 additional vacuum layers. For the heterostructures, we consider 11 atomic layers of each of the two materials. A kinetic energy cutoff of 520 eV is used for all (bulk, surface, and interface) calculations. The Brillouin Zones (BZ) are sampled using Γ -centered Monkhorst-Pack (MP) grid with $15 \times 15 \times 15$ *k*-points for bulk and $15 \times 15 \times 1$ *k*-points for surface and interface calculations. The atomic relaxations are performed until the Hellmann-Feynman forces on atoms are reduced to less than 0.001 eV/Å. We do not consider dipole corrections as all the considered surfaces are nonpolar.

For all the considered methods, bulk, surface, and interface calculations are carried out using the r²SCAN-optimized geometries and ionic positions. Note that the r²SCAN geometries are very accurate for bulk crystals, being much closer to experimental values than PBE ones⁶².

For the construction of the heterostructure supercell, we follow the method of Refs. 39 and 76. For the in-plane lattice parameter we take the average value of the bulk lattice parameters (r²SCAN-optimized) of the two materials forming the (110) interface. After that, the out-of-plane lattice parameter and internal coordinates of the heterostructure are allowed to relax at the fixed in-plane parameters. This means that the bulk-like regions in the A and B parts of the supercell do not agree with the cubic bulk structures of materials A and B. Therefore, to evaluate Eq. (5) for bulk calculations we consider tetragonally strained unit cell that agrees with crystal structures in the bulk-like regions of the supercell. In this case we will refer strained band offset.

Spin-orbit coupling is considered in the bulk calculations only since its inclusion in surface and interface calculations has almost no influence on the electrostatic potential.

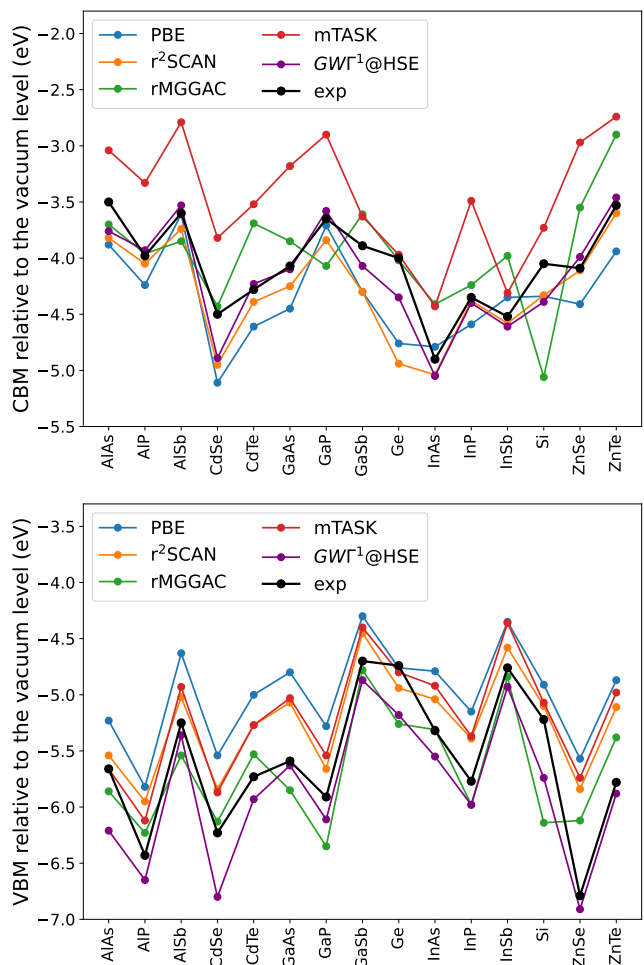


FIG. 1. CBMs relative to the vacuum level (negative of the EAs) and VBMs relative to the vacuum level (negative of the IPs) as obtained from different levels of theory. The IPs were calculated with Eq. (1) and EAs with $\epsilon_{EA} = \epsilon_{IP} - \epsilon_g$, where ϵ_g is the band gap. For comparison, we also show the experimental and GW¹@HSE results from Ref. 39. Numerical values are given in Table S1 of the Supplementary Material⁹².

E. Analysis of results

1. IP, EA, and Band gaps

In Figs. 1 and 2 we compare the position of the VBM and CB minima (CBM) with respect to the vacuum level calculated for the (110) surfaces and the bulk band gaps, respectively, using the PBE GGA functional and different meta-GGA functionals (r²SCAN, rMGGAC, mTASK, and LMBJ). For comparison, we also present the experimental results as well as those from GW¹@HSE calculations from Ref. 39. We note that the GW¹@HSE results reported in Ref. 39 may be considered the best available theoretical prediction for the electronic properties of the semiconductors. Therefore, we will use these throughout this paper as a reference for comparison with

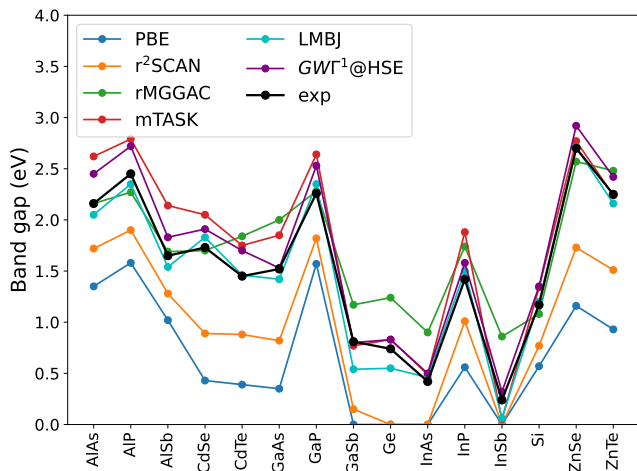


FIG. 2. Bulk band gaps as obtained from different levels of theory with spin-orbit coupling included. For comparison, we also show the experimental and $\text{GW}\Gamma^1\text{@HSE}$ results from Ref. 39. All numerical values are given in Table S1 of the Supplementary Material⁹².

other functionals we studied. All the calculated values are summarized in Table S1 of the Supplementary Material⁹².

Analyzing the results obtained from different semilocal XC methods, we observe that the standard GGA PBE functional shows the largest deviation from the experimental and $\text{GW}\Gamma^1\text{@HSE}$ values for the VBMs and band gaps of group II-VI semiconductors. On the other hand, CBMs are better reproduced by this method. Therefore, one can expect that the underestimation of the band gaps (shown in Fig. 2) obtained using the PBE functional mainly comes from the deviations from the VBMs. In general, we can conclude that PBE places the VBMs too high and CBMs slightly low in energy, leading to an overall underestimated band gap. This observation is consistent with what reported in Ref. 39. Nevertheless, a better representation of VBMs from PBE may be obtained using the $\text{PBE}-\frac{1}{2}$ ^{193,94}, or the GLLB-sc⁹⁵ techniques, where the orbital information and/or derivative discontinuities are taken into account explicitly^{94,95}.

Now, we come to the performance of the meta-GGA functionals $r^2\text{SCAN}$, $r\text{MGGAC}$, and $m\text{TASK}$. For $r^2\text{SCAN}$ and $m\text{TASK}$, the behavior is similarly to that of PBE. Both functionals underestimate the IPs, but by a lesser margin. Finally, $r\text{MGGAC}$ yields the smallest average error with respect to the experimental and $\text{GW}\Gamma^1\text{@HSE}$ values. No clear trend can be deduced, as the IPs are in this case overestimated for some materials and underestimated for others. For the CBMs, we observe a different behavior. $r^2\text{SCAN}$ places the CBMs slightly low, similar to PBE. $m\text{TASK}$, on the other hand, predicts too high a position of the CBMs, due to its overall overestimation of the bulk band gaps. For $r\text{MGGAC}$, again, no clear trend can be identified, as some CBMs are placed too high in energy and others low. Finally, look-

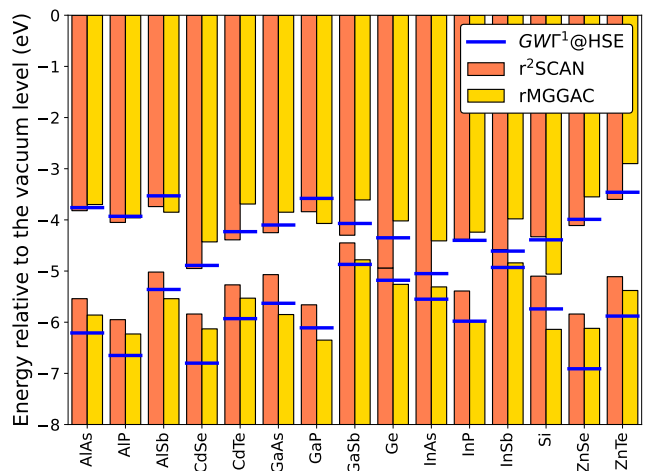


FIG. 3. Band alignment based on the IPs (negatives of the VBM to the vacuum level) and EAs (negatives of CBM to the vacuum level) as obtained using $r^2\text{SCAN}$ (red) and $r\text{MGGAC}$ (yellow), compared with reference $\text{GW}\Gamma^1\text{@HSE}$ values (blue) from Ref. 39. All the surface orientations are along (110) directions.

ing at the band gaps (Fig. 2), we see that overall LMBJ yields the most accurate band gaps, which is inherited from the original MBJ potential. This is in agreement with previous studies^{32,96}. $m\text{TASK}$ and $r\text{MGGAC}$ predict slightly too wide band gaps, whereas $r^2\text{SCAN}$ yields too narrow ones, similar to PBE.

In addition, the improved VBM positions from $r\text{MGGAC}$ are also very much evident from Fig. 3, where the $\text{GW}\Gamma^1\text{@HSE}$ reference values³⁹ are added for comparison. However, the CBMs are slightly underestimated for most of the systems considering the $\text{GW}\Gamma^1\text{@HSE}$ benchmark reference³⁹. For $r^2\text{SCAN}$, on the other hand, we see the systematic overestimation of the VBM position, whereas the CBM position agrees much better with the $\text{GW}\Gamma^1\text{@HSE}$ reference.

2. Band offsets

Here, we finally discuss the valence band offsets (VBO) obtained by the three methods: IP-based, BPE-based, average potential based. The VBOs obtained from the IPs and BPEs using different meta-GGA semilocal XC functionals for chosen 14 pairs of semiconductors with small lattice mismatch are reported in Table S3 of the Supplementary Material⁹² and those obtained by the APM are listed in Table I. For convenience, the BPEs from different XC functionals are also reported in Table S2 of the Supplementary Material⁹². For comparison, we show all the individual results compared with the $\text{GW}\Gamma^1\text{@HSE}$ results in Fig. 4. It should be noted that the reference results were obtained for slightly different supercell models in Ref. 39. In that work, the natural band offsets were calculated, for which the bulk VBM position

TABLE I. Strained band offsets (in eV) as calculated using the average potential method. The natural band offsets calculated with $\text{GW}\Gamma^1\text{@HSE}$ are from Ref. 39.

| Interfaces | Mismatch | PBE | $r^2\text{SCAN}$ | rMGGAC | MTASK | LMBJ | $\text{GW}\Gamma^1\text{@HSE}$ |
|------------|----------|-------|------------------|--------|-------|-------|--------------------------------|
| ZnTe/AlSb | 1.09 | -0.36 | -0.41 | -0.41 | -0.36 | -0.44 | -0.59 |
| Si/GaP | 0.26 | 0.30 | 0.35 | 0.45 | 0.36 | 0.35 | 0.51 |
| InSb/CdTe | 0.11 | 0.48 | 0.57 | 0.67 | 0.75 | 0.68 | 0.86 |
| InP/InAs | 3.35 | -0.34 | -0.40 | -0.40 | -0.49 | -0.47 | -0.35 |
| Ge/ZnSe | 0.18 | 1.14 | 1.32 | 1.18 | 1.36 | 1.46 | 1.85 |
| Ge/AlAs | 0.07 | 1.02 | 1.16 | 1.05 | 1.35 | 1.12 | 1.19 |
| GaSb/AlSb | 0.74 | 0.34 | 0.39 | 0.36 | 0.52 | 0.38 | 0.48 |
| GaP/AlP | 0.34 | 0.49 | 0.53 | 0.46 | 0.66 | 0.44 | 0.58 |
| GaAs/ZnSe | 0.03 | 0.70 | 0.80 | 0.74 | 0.81 | 0.89 | 1.25 |
| GaAs/InP | 3.99 | 0.25 | 0.26 | 0.25 | 0.22 | 0.32 | 0.43 |
| GaAs/Ge | 0.21 | -0.42 | -0.53 | -0.45 | -0.59 | -0.59 | -0.56 |
| GaAs/AlAs | 0.14 | 0.47 | 0.52 | 0.49 | 0.65 | 0.45 | 0.55 |
| CdSe/ZnTe | 0.44 | -0.66 | -0.71 | -0.81 | -0.95 | -0.81 | -0.92 |
| GaSb/ZnTe | 0.36 | 0.57 | 0.68 | 0.63 | 0.72 | 0.73 | 0.96 |

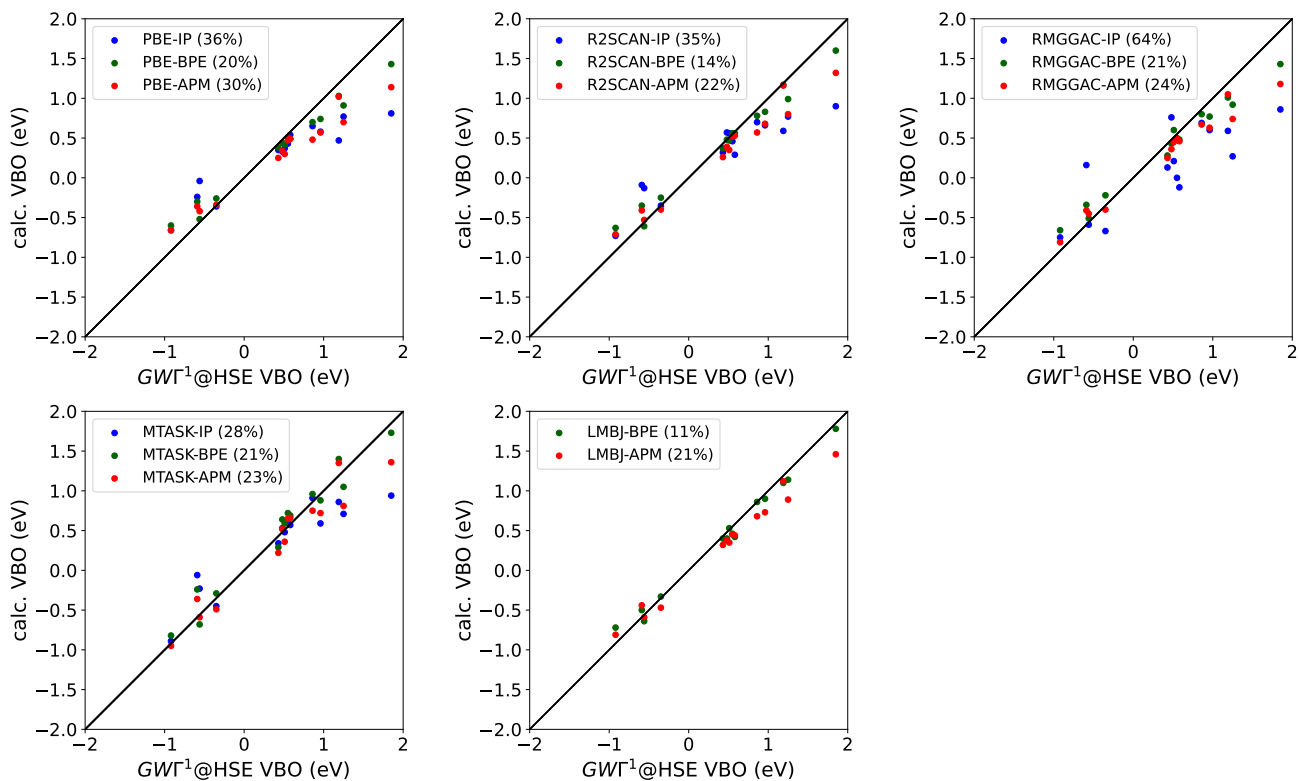


FIG. 4. PBE and meta-GGA vs $\text{GW}\Gamma^1\text{@HSE}$ VBOs for the set of 14 heterostructure interfaces calculated with the IP-, BPE-, and average potential based methods. The $\text{GW}\Gamma^1\text{@HSE}$ results are from Ref. 39. In the legends of each panel, the values of the mean absolute percentage error are given.

with respect to the bulk reference level was evaluated at the equilibrium bulk structure, and the VBOs were then further corrected by calculating the shift of the VBM with strain. The latter was evaluated from additional surface calculations. Here, we consider only interfaces of materials with a small lattice mismatch. Since we found a quite unsatisfying performance of the IP-based approach obtained by surface calculations, as shown be-

low, we chose to evaluate the strained VBOs instead. For perfectly lattice matched materials both results would be identical, and we expect the discrepancy to remain small for our subset of interfaces. We, therefore, consider such comparison more meaningful than with experimental results, for which details of the atomic structure of the interface are often unknown.

The first and most remarkable finding is the fact that

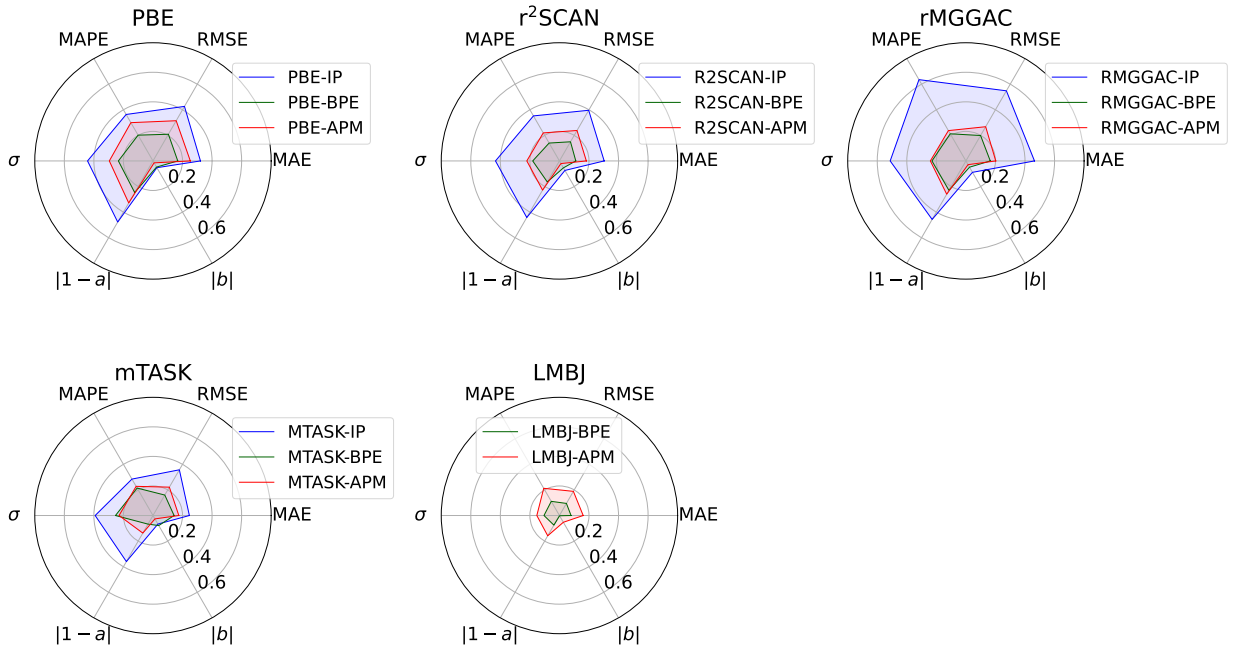


FIG. 5. Radar plots showing the statistical quantities MAPE, RMSE (in eV), MAE (in eV), standard deviation (σ , in eV), and the parameters a and b (in eV) from the fit ($y = ax + b$) to the theoretical $\text{GWT}^1\text{@HSE}$ values in Fig. 4 for all XC functionals.

the BPE method yields overall the best results, despite being the numerically cheapest one. This is partially attributed to the choice of semiconductors that have quite similar structures and only a small lattice mismatch. In such situations, the quality of the description of the bulk electronic structure in the vicinity of the VBM and CBM becomes important. It is thus not surprising that LMBJ yields the best result here (mean absolute percentage error (MAPE) of 11%), since the original MBJ was shown to predict the band gaps with high accuracy^{32,96}, closely followed by $r^2\text{SCAN}$ (MAPE of 14%). $r\text{MGGAC}$ and $m\text{TASK}$ perform similarly to PBE when the BPE-based method is used (MAPE of $\sim 21\%$).

We also obtain fairly good results from the APM for all the tested meta-GGAs $r^2\text{SCAN}$, $r\text{MGGAC}$, $m\text{TASK}$, and LMBJ, with MAPE slightly above 20%, performing better than PBE-APM (MAPE of 30%). It should be noted that in presence of larger lattice mismatch, interface reconstructions, and other inhomogeneities, the APM is expected to be the most accurate since it is the only one that takes into account the details of the interface.

Finally, the worst results overall are obtained using the IP-based method. Only for $m\text{TASK}$, the MAPE is moderate (26 %). $r^2\text{SCAN}$ yields VBOs with the same accuracy as PBE (MAPE of $\sim 35\%$). Interestingly, we obtained the worst result for $r\text{MGGAC}$ with the IP-based method (MAPE of 64 %), even though the individual IPs were calculated with the best accuracy with this functional. The systematic underestimation of the IPs in

the case of PBE and $r^2\text{SCAN}$ works favorably here when compared with $r\text{MGGAC}$.

To further quantify the quality of the chosen meta-GGA functionals for the calculation of VBOs, we plot the statistical quantities MAPE, root mean square error (RMSE), mean absolute error (MAE), standard deviation (σ) in Fig. 5, and the parameters a and b from the fit to the theoretical $\text{GWT}^1\text{@HSE}$ values in Fig. 4.

Roughly from the radar plots, it can be understood that the smaller the area, the better the performance of the method. This analysis further confirms our overall results. The IP-based method is the worst in all cases. On the other hand, the BPE-based method and the APM performs fairly similarly. Moreover, $r^2\text{SCAN}$, $r\text{MGGAC}$, $m\text{TASK}$, and LMBJ all outperform PBE. However, it should be kept in mind that we only studied rather ideal interfaces of similar semiconductors with VBM and CBM with mainly s - and p -character. Larger deviations of these two methods for heterostructures involving highly localized d -electrons close to the Fermi energy and interfaces with larger lattice mismatch are possible. In particular, it is known that MBJ and LMBJ are sometimes not very accurate for the band gap of non-magnetic systems with d -electrons (e.g., Cu_2O ^{96,97}) and we expect that this can also influence the VBO.

IV. CONCLUSIONS

Since accurate GW calculations for band offsets using the APM and sometimes even with the IP- and BPE-based methods might be too expensive, as an alternative, we show that modern meta-GGA functionals may be the choice for the calculation of band offsets in heterostructure systems. In summary, we have shown that the performance of the meta-GGA functionals is quite promising and reliable in calculating the band offsets. Overall analysis shows that PBE, r^2 SCAN, and mTASK provide too high VBM positions (underestimates IPs), while mostly agreeing well for the CBMs (or EAs), with the exception of mTASK, which puts the CBMs too high in energy. rMGGAC results agree quite well for VBMs and CBMs, but no clear trend was observed, as some of the band edges are overestimated and some are underestimated. For the chosen test set of semiconductor heterostructures with small lattice mismatch, we observed improved performance of the meta-GGA functionals in comparison with PBE. For all meta-GGAs, the BPE-based method yields the smallest error with respect to theoretical $\text{GWT}^1\text{@HSE}$ values from Ref. 39. The error from the APM is found to slightly higher than that from BPE method. Finally, the IP-based method proved successful only in the case of mTASK.

For most of the interfaces, we obtain a good agreement of the VBOs from r^2 SCAN, rMGGAC, mTASK, and LMBJ. Furthermore, our comparison of the VBOs obtained from BPE and APM shows that in most cases all these methods give quantitatively reasonable results and a possible alternative to the expensive GW calculation. We hope that the present study will stimulate further benchmark comparative studies of heterogeneous systems forming a common interface, as well as for interfaces of 2D systems, a growing topic of present day electronic structure theory.

SUPPLEMENTARY MATERIAL

See the supplementary material for the complete results reported in this paper.

ACKNOWLEDGMENTS

A.G. would like to thank INSPIRE fellowship, DST, India for financial support. T.T. and S.B. acknowledge funding from the Volkswagen Stiftung (Momentum) through the “Dandelion” project. M.K.N acknowledges support from DST-FIST(SR/FST/PSI-215/2016).

DATA AVAILABILITY

The data that supports the findings of this study are available within the article and its supplementary mate-

rial.

- ¹A. Facchetti and T. J. Marks, “Transparent electronics: From synthesis to applications,” in *Transparent electronics: From synthesis to applications* (John Wiley & Sons Ltd, Chichester, 2010).
- ²A. Franciosi and C. G. Van de Walle, *Surf. Sci. Rep.* **25**, 1 (1996).
- ³I. Vurgaftman, J. R. Meyer, and L. R. Ram-Mohan, *J. Appl. Phys.* **89**, 5815 (2001).
- ⁴W. Mönch, “Electronic properties of semiconductor interfaces,” in *Springer Handbook of Electronic and Photonic Materials*, edited by S. Kasap and P. Capper (Springer International Publishing, Cham, 2017) pp. 1–1.
- ⁵J. Robertson, *J. Vac. Sci. Technol. A* **31**, 050821 (2013).
- ⁶Z. I. Alferov, *Rev. Mod. Phys.* **73**, 767 (2001).
- ⁷J. A. del Alamo, *Nature* **479**, 317 (2011).
- ⁸W. A. Harrison, E. A. Kraut, J. R. Waldrop, and R. W. Grant, *Phys. Rev. B* **18**, 4402 (1978).
- ⁹N. Nakagawa, H. Y. Hwang, and D. A. Muller, *Nat. Mater.* **5**, 204 (2006).
- ¹⁰Y. Ikebe, T. Morimoto, R. Masutomi, T. Okamoto, H. Aoki, and R. Shimano, *Phys. Rev. Lett.* **104**, 256802 (2010).
- ¹¹A. V. Stier, C. T. Ellis, J. Kwon, H. Xing, H. Zhang, D. Eason, G. Strasser, T. Morimoto, H. Aoki, H. Zeng, B. D. McCombe, and J. Cerne, *Phys. Rev. Lett.* **115**, 247401 (2015).
- ¹²V. Dziom, A. Shuvaev, A. V. Shchepetilnikov, D. MacFarland, G. Strasser, and A. Pimenov, *Phys. Rev. B* **99**, 045305 (2019).
- ¹³J. Anversa, P. Piquini, A. Fazzio, and T. M. Schmidt, *Phys. Rev. B* **90**, 195311 (2014).
- ¹⁴B. A. Bernevig, T. L. Hughes, and S.-C. Zhang, *Science* **314**, 1757 (2006).
- ¹⁵M. König, S. Wiedmann, C. Brüne, A. Roth, H. Buhmann, L. W. Molenkamp, X.-L. Qi, and S.-C. Zhang, *Science* **318**, 766 (2007).
- ¹⁶C. G. Van de Walle, *Phys. Rev. B* **39**, 1871 (1989).
- ¹⁷W. R. Frensley and H. Kroemer, *Phys. Rev. B* **16**, 2642 (1977).
- ¹⁸C. Tejedor and F. Flores, *J. Phys. C: Solid State Phys.* **11**, L19 (1977).
- ¹⁹W. E. Pickett, S. G. Louie, and M. L. Cohen, *Phys. Rev. B* **17**, 815 (1978).
- ²⁰C. G. Van de Walle and R. M. Martin, *Phys. Rev. B* **35**, 8154 (1987).
- ²¹P. Hohenberg and W. Kohn, *Phys. Rev.* **136**, B864 (1964).
- ²²W. Kohn and L. J. Sham, *Phys. Rev.* **140**, A1133 (1965).
- ²³E. Engel and R. M. Dreizler, *Density functional theory* (Springer, 2013).
- ²⁴K. Burke, *J. Chem. Phys.* **136**, 150901 (2012).
- ²⁵R. O. Jones, *Rev. Mod. Phys.* **87**, 897 (2015).
- ²⁶J. P. Perdew and Y. Wang, *Phys. Rev. B* **45**, 13244 (1992).
- ²⁷J. P. Perdew, K. Burke, and Y. Wang, *Phys. Rev. B* **54**, 16533 (1996).
- ²⁸J. P. Perdew, A. Ruzsinszky, G. I. Csonka, O. A. Vydrov, G. E. Scuseria, L. A. Constantin, X. Zhou, and K. Burke, *Phys. Rev. Lett.* **100**, 136406 (2008).
- ²⁹L. Weston, H. Taylor, K. Krishnaswamy, L. Bjaalie, and C. Van de Walle, *Comput. Mater. Sci.* **151**, 174 (2018).
- ³⁰J. P. Perdew, W. Yang, K. Burke, Z. Yang, E. K. U. Gross, M. Scheffler, G. E. Scuseria, T. M. Henderson, I. Y. Zhang, A. Ruzsinszky, H. Peng, J. Sun, E. Trushin, and A. Görling, *Proc. Natl. Acad. Sci. U. S. A.* **114**, 2801 (2017).
- ³¹F. Tran, P. Blaha, and K. Schwarz, *J. Phys.: Condens. Matter* **19**, 196208 (2007).
- ³²P. Borlido, J. Schmidt, A. W. Huran, F. Tran, M. A. L. Marques, and S. Botti, *NPJ Comput. Mater.* **6**, 96 (2020).
- ³³B. Patra, S. Jana, L. A. Constantin, and P. Samal, *Phys. Rev. B* **100**, 045147 (2019).
- ³⁴F. Tran, S. Ehsan, and P. Blaha, *Phys. Rev. Materials* **2**, 023802 (2018).
- ³⁵S. Jana, K. Sharma, and P. Samal, *J. Chem. Phys.* **149**, 164703 (2018).
- ³⁶S. Jana, A. Patra, and P. Samal, *J. Chem. Phys.* **149**, 044120 (2018).

- ³⁷F. Tran and P. Blaha, *J. Phys. Chem. A* **121**, 3318 (2017).
- ³⁸F. Tran, J. Doumont, L. Kalantari, A. W. Huran, M. A. L. Marques, and P. Blaha, *J. Appl. Phys.* **126**, 110902 (2019).
- ³⁹Y. Hinuma, A. Grüneis, G. Kresse, and F. Oba, *Phys. Rev. B* **90**, 155405 (2014).
- ⁴⁰A. Grüneis, G. Kresse, Y. Hinuma, and F. Oba, *Phys. Rev. Lett.* **112**, 096401 (2014).
- ⁴¹J. Heyd, G. E. Scuseria, and M. Ernzerhof, *J. Chem. Phys.* **118**, 8207 (2003).
- ⁴²A. V. Krugau, O. A. Vydrov, A. F. Izmaylov, and G. E. Scuseria, *J. Chem. Phys.* **125**, 224106 (2006).
- ⁴³J. Heyd and G. E. Scuseria, *J. Chem. Phys.* **121**, 1187 (2004).
- ⁴⁴S. Jana and P. Samal, *Phys. Chem. Chem. Phys.* **21**, 3002 (2019).
- ⁴⁵S. Jana, A. Patra, L. A. Constantin, and P. Samal, *J. Chem. Phys.* **152**, 044111 (2020).
- ⁴⁶S. Jana, B. Patra, S. Śmiga, L. A. Constantin, and P. Samal, *Phys. Rev. B* **102**, 155107 (2020).
- ⁴⁷H. Zheng, M. Govoni, and G. Galli, *Phys. Rev. Materials* **3**, 073803 (2019).
- ⁴⁸N. P. Brawand, M. Vörös, M. Govoni, and G. Galli, *Phys. Rev. X* **6**, 041002 (2016).
- ⁴⁹N. P. Brawand, M. Govoni, M. Vörös, and G. Galli, *J. Chem. Theory Comput.* **13**, 3318 (2017).
- ⁵⁰W. Chen, G. Miceli, G.-M. Rignanese, and A. Pasquarello, *Phys. Rev. Materials* **2**, 073803 (2018).
- ⁵¹Z.-H. Cui, Y.-C. Wang, M.-Y. Zhang, X. Xu, and H. Jiang, *J. Phys. Chem. Lett.* **9**, 2338 (2018).
- ⁵²S. Jana, L. A. Constantin, S. Śmiga, and P. Samal, *J. Chem. Phys.* **157**, 024102 (2022).
- ⁵³L. Hedin, *Phys. Rev.* **139**, A796 (1965).
- ⁵⁴M. S. Hybertsen and S. G. Louie, *Phys. Rev. B* **34**, 5390 (1986).
- ⁵⁵Z. Zhang, Y. Guo, H. Lu, S. J. Clark, and J. Robertson, *Appl. Phys. Lett.* **116**, 131602 (2020).
- ⁵⁶T. Bischoff, I. Reshetnyak, and A. Pasquarello, *Phys. Rev. B* **101**, 235302 (2020).
- ⁵⁷P. Borlido, M. A. L. Marques, and S. Botti, *J. Chem. Theory Comput.* **14**, 939 (2018).
- ⁵⁸J. P. Perdew, A. Ruzsinszky, G. I. Csonka, L. A. Constantin, and J. Sun, *Phys. Rev. Lett.* **103**, 026403 (2009).
- ⁵⁹J. Sun, A. Ruzsinszky, and J. P. Perdew, *Phys. Rev. Lett.* **115**, 036402 (2015).
- ⁶⁰D. Mejia-Rodriguez and S. Trickey, *Phys. Rev. B* **98**, 115161 (2018).
- ⁶¹B. Patra, S. Jana, L. A. Constantin, and P. Samal, *Phys. Rev. B* **100**, 155140 (2019).
- ⁶²J. W. Furness, A. D. Kaplan, J. Ning, J. P. Perdew, and J. Sun, *J. Phys. Chem. Lett.* **11**, 8208 (2020).
- ⁶³S. Jana, S. K. Behera, S. Śmiga, L. A. Constantin, and P. Samal, *New J. Phys.* (2021).
- ⁶⁴B. Neupane, H. Tang, N. K. Nepal, S. Adhikari, and A. Ruzsinszky, *Phys. Rev. Materials* **5**, 063803 (2021).
- ⁶⁵T. Aschebrock and S. Kümmel, *Phys. Rev. Res.* **1**, 033082 (2019).
- ⁶⁶F. Della Sala, E. Fabiano, and L. A. Constantin, *Int. J. Quantum Chem.* **22**, 1641 (2016).
- ⁶⁷A. Patra, S. Jana, L. A. Constantin, and P. Samal, *J. Chem. Phys.* **153**, 084117 (2020).
- ⁶⁸A. Patra, S. Jana, P. Samal, F. Tran, L. Kalantari, J. Doumont, and P. Blaha, *J. Phys. Chem. C* **125**, 11206 (2021).
- ⁶⁹F. Tran, J. Doumont, L. Kalantari, P. Blaha, T. Rauch, P. Borlido, S. Botti, M. A. L. Marques, A. Patra, S. Jana, and P. Samal, *J. Chem. Phys.* **155**, 104103 (2021).
- ⁷⁰J. Tersoff, *Phys. Rev. B* **30**, 4874 (1984).
- ⁷¹J. Tersoff, *Phys. Rev. B* **32**, 6968 (1985).
- ⁷²A. Schleife, F. Fuchs, C. Rödl, J. Furthmüller, and F. Bechstedt, *Appl. Phys. Lett.* **94**, 012104 (2009).
- ⁷³W. Mönch, *J. Appl. Phys.* **80**, 5076 (1996).
- ⁷⁴Y. Guo and J. Robertson, *Phys. Rev. Materials* **1**, 044004 (2017).
- ⁷⁵Y. Guo, H. Li, S. J. Clark, and J. Robertson, *J. Phys. Chem. C* **123**, 5562 (2019).
- ⁷⁶Y. Hinuma, F. Oba, Y. Kumagai, and I. Tanaka, *Phys. Rev. B* **88**, 035305 (2013).
- ⁷⁷B. Höffling, A. Schleife, C. Rödl, and F. Bechstedt, *Phys. Rev. B* **85**, 035305 (2012).
- ⁷⁸T. Rauch, M. A. L. Marques, and S. Botti, *J. Chem. Theory Comput.* **16**, 2654 (2020).
- ⁷⁹F. Tran and P. Blaha, *Phys. Rev. Lett.* **102**, 226401 (2009).
- ⁸⁰J. Tao, J. P. Perdew, V. N. Staroverov, and G. E. Scuseria, *Phys. Rev. Lett.* **91**, 146401 (2003).
- ⁸¹B. Patra, S. Jana, L. A. Constantin, and P. Samal, *J. Phys. Chem. C* **125**, 4284 (2021).
- ⁸²A. D. Becke and E. R. Johnson, *J. Chem. Phys.* **124**, 221101 (2006).
- ⁸³D. Koller, F. Tran, and P. Blaha, *Phys. Rev. B* **85**, 155109 (2012).
- ⁸⁴T. Rauch, M. A. L. Marques, and S. Botti, *Phys. Rev. B* **102**, 119902 (2020).
- ⁸⁵T. Rauch, M. A. L. Marques, and S. Botti, *J. Chem. Theory Comput.* **17**, 4746 (2021).
- ⁸⁶A. M. Cowley and S. M. Sze, *J. Appl. Phys.* **36**, 3212 (1965).
- ⁸⁷S.-H. Wei and A. Zunger, *Phys. Rev. Lett.* **59**, 144 (1987).
- ⁸⁸G. Kresse and J. Hafner, *Phys. Rev. B* **47**, 558 (1993).
- ⁸⁹G. Kresse and J. Furthmüller, *Phys. Rev. B* **54**, 11169 (1996).
- ⁹⁰G. Kresse and D. Joubert, *Phys. Rev. B* **59**, 1758 (1999).
- ⁹¹G. Kresse and J. Furthmüller, *Comput. Mater. Sci.* **6**, 15 (1996).
- ⁹²“Supplementary Material.”
- ⁹³L. G. Ferreira, M. Marques, and L. K. Teles, *AIP Advances* **1**, 032119 (2011).
- ⁹⁴J. Doumont, F. Tran, and P. Blaha, *Phys. Rev. B* **99**, 115101 (2019).
- ⁹⁵F. Tran, S. Ehsan, and P. Blaha, *Phys. Rev. Materials* **2**, 023802 (2018).
- ⁹⁶P. Borlido, T. Aull, A. W. Huran, F. Tran, M. A. L. Marques, and S. Botti, *J. Chem. Theory Comput.* **15**, 5069 (2019).
- ⁹⁷T. Rauch, M. A. L. Marques, and S. Botti, *Phys. Rev. B* **101**, 245163 (2020).